A Climatology of Lee Cyclones across the Central United States, 1980–2021

McKENZIE L. LARSON [a] AND ANDREW C. WINTERS[a]

[a] Department of Atmospheric and Oceanic Sciences, University of Colorado Boulder, Boulder, Colorado

ABSTRACT: The central United States is a favorable region for cyclogenesis east of the Rocky Mountains. This region's distinctive location in the center of the continental United States and juxtaposition with complex topography contribute to unique forecast challenges, including uncertainties in the prediction of extratropical cyclone (ETC) intensity and location, as well as concomitant areas of heavy precipitation and strong winds. Consequently, this study utilizes machine learning techniques to investigate the variability of cold-season (October–May) ETC characteristics across the central United States. ETCs are identified within the fifth generation European Centre for Medium-Range Weather Forecasts (ECMWF) atmospheric reanalysis (ERA5) during 1980–2021 using a method for ETC detection adopted from previously published work. This ETC dataset subsequently facilitates an analysis of the monthly and seasonal frequency of central U.S. ETCs, for which an increase in cold-season ETC frequency is found for both winter and springtime ETCs. A self-organizing map (SOM) is trained on mean sea level pressure anomalies from ERA5 during ETC events and used to examine the variability in large-scale weather regimes conducive to central U.S. ETCs. These regimes are categorized into five clusters: 1) the Mississippi River anticyclone, 2) the Canadian anticyclone, 3) the Northern Plains cyclone, 4) the Central Plains cyclone, and 5) the Southern Plains cyclone clusters. One main finding is a significant increase of ETCs that are categorized into the Canadian anticyclone cluster, indicating that a subset of weaker central U.S. ETCs are becoming more common. The extent to which the characteristics of near-ETC environments (e.g., moisture sources, upper-level jet stream structure, quasigeostrophic ascent, and precipitation) vary as a function of each SOM cluster is also investigated.

SIGNIFICANCE STATEMENT: Extratropical cyclones frequently produce strong precipitation and winds across the central United States, resulting in profound societal impacts. This study investigates the various atmospheric environments (e.g., moisture sources, upper-level jet stream structure, and precipitation) that accompany cyclone development in this region. Machine learning methods are used to identify distinct categories of cyclone events, and the different upper- and lower-level environments associated with these cyclone categories are explored. We find that while central U.S. ETCs have been increasing during 1980–2021, weaker ETCs associated with higher pressures and less moisture are particularly becoming more common.

KEYWORDS: Extratropical cyclones; Synoptic climatology; Synoptic-scale processes; Winter/cool season; Machine learning

---

1. Introduction

Extratropical cyclones (ETCs) are synoptic-scale weather systems that frequently characterize cool-season (October–May) weather patterns at midlatitudes. In North America, ETCs are frequently observed throughout Canada and the United States, with three distinct genesis regions for ETCs that most often lead to extreme weather events (i.e., ETCs that cause large societal disturbances, impact broad geographic regions, are climatologically infrequent, and take place over an extended period of time; Bentley et al. 2019). These genesis regions include areas leeward of the Rocky Mountains, over the south-central United States, and along the east coast of North America. Fritzen et al. (2021) further defined various North

American ETC genesis clusters, such as Colorado lows, Bighorn lows (Wyoming/Montana), and Alberta lows near the Rocky Mountains; the Superior low near the Great Lakes; and East Coast and Labrador lows near the east coast of North America. Near the Rocky Mountains, the formation of an ETC downwind of a mountain range, or lee cyclogenesis, represents one of the predominant mechanisms for cyclogenesis across the central United States (Newton 1956). In particular, vortex stretching in the presence of an upper-level trough can facilitate the formation of ETCs in the lee of the Rocky Mountains in collaboration with the production of low-level cyclonic vorticity that accompanies downslope flow downstream of the orography (Palmén and Newton 1969; Bannon 1992; Davis 1997).

Strong winds and vast amounts of precipitation are often produced in association with ETCs, which can result in societal impacts. The 13–14 March 2021 Northeast Colorado Blizzard (NWS 2024) produced 17.4 in. (44.2 cm) of snow in the Denver, Colorado, metro area, with snowfall totals exceeding 3 ft (91 cm) in foothills locations west of Fort Collins, Colorado. This ETC slowed and strengthened as it migrated from the southwest United States toward eastern Colorado. Snow production was

Corresponding author: McKenzie L. Larson, mckenzie.larson@colorado.edu

amplified by the ETC's cyclonic circulation, which produced strong easterly upslope flow along the Colorado Front Range. This upslope flow was further enhanced by the development of a barrier jet, in which cold air accelerates equatorward along the leeward side of the Colorado Front Range (Dunn 1987, 1992). Barrier jets are produced when easterly winds associated with the ETC are deflected equatorward once they encounter the orography. Cold air anomalies within the barrier jet are also further enhanced by diabatic cooling from melting and evaporating hydrometeors. The presence of a barrier jet broadens the effect of orographic lift by initiating the strongest upslope flow farther eastward of the immediate foothills, increasing precipitation rates within the Denver metro area. The 13–14 March 2021 Northeast Colorado Blizzard is just one example of an impactful ETC that formed via lee cyclogenesis downwind of the Rocky Mountains. The full spectrum of central U.S. ETCs exhibits unique and varied interactions with local orography, occasionally resulting in powerful ETCs. With dense and growing population centers across the central United States (Bureau 2024), ETCs in this region require additional study to improve our understanding and prediction of these events, as well as their variability.

As demonstrated by the 13–14 March 2021 Northeast Colorado Blizzard, central U.S. ETCs feature complex interactions with the Rocky Mountains. In contrast to its interaction with a barrier jet, the cyclonic flow associated with ETCs near orography can also lead to enhanced downslope flow within the equatorward sector of the ETC via the descent of westerly flow east of the mountain range. This descent, combined with the midlevel ascent induced ahead of a shortwave trough, can enhance vortex stretching and increase low-level cyclonic vorticity east of the orography (Clark 1990). Downslope flow not only facilitates lee cyclogenesis but also produces adiabatic warming and drying of air masses. This subsiding dry air mass can subsequently develop into a dry intrusion (Browning 1997), enhancing dry air and warm anomalies that can be observed near and to the south of the ETC center. Considered together, the presence of downslope flow east of the Rocky Mountains provides increased subsidence that not only strengthens the cyclonic circulation of ETCs but also hinders the production of precipitation within the warm and dry air mass that is often produced in the vicinity of the developing lee cyclone.

North American ETC climatologies highlight the formation of Bighorn lows near the Montana/Wyoming border and Colorado lows in eastern Colorado as being particularly relevant to the climate variability of the central United States (Whittaker and Horn 1981; Fritzen et al. 2021). While many regional ETC climatologies exist and are occasionally modernized, extensive ETC climatologies focused on the central United States, and specifically Colorado lows, have not been updated since the 1990s (Fawcett and Saylor 1965; Marshment and Horn 1986; Bierly and Harrington 1995). This study is particularly novel because of the recent advent of state-of-the-art reanalysis products, such as the fifth generation European Centre for Medium-Range Weather Forecasts (ECMWF) atmospheric reanalysis (ERA5; Hersbach et al. 2023), which enable a climatological examination of cyclone characteristics at finer temporal and spatial resolution than ever before. Prior cyclone climatologies primarily examine temporal trends in ETC frequency to determine how ETC counts and their minimum pressure values have evolved over time. This study develops an updated central U.S. ETC climatology, which includes both temporal and spatial statistics, to investigate how central U.S. ETCs are changing in both frequency and location. Furthermore, this climatology utilizes ETC-centered composites and machine learning to discern how central U.S. ETC environments vary across events, allowing for a better understanding of ETC characteristics that extends beyond bulk seasonal statistics. The categorization of ETCs using machine learning techniques further facilitates an investigation into how the variability in ETC characteristics translates to different sensible weather impacts across the central United States via the spectrum of interactions ETCs can have with local orography.

The remainder of this paper is structured as follows. Section 2 introduces the methodology used to identify central U.S. cyclones. Section 3 describes the temporal and spatial statistics for cool-season central U.S. ETCs during 1980–2021. Section 4 introduces a self-organizing map algorithm that is used to identify unique central U.S. ETC characteristics based on the varied distribution of mean sea level pressure (MSLP) anomalies across events. Section 5 summarizes the results from sections 3 and 4, contextualizes this ETC climatology with previous literature, and offers considerations for future work.

2. Lee cyclone identification

This study uses data at 1-h intervals during October–May 1980–2021 from ERA5 (Hersbach et al. 2023). ERA5 data feature 0.25° × 0.25° horizontal grid spacing and 37 isobaric levels extending from 1000 to 1 hPa. Summer months are excluded from this analysis to focus on synoptically driven cyclones during the cool season. Bierly and Harrington (1995) excluded September in their study since the number of hemispheric waves during this month is more characteristic of summer atmospheric flow patterns (Harman 1991). The decision to exclude September in this study is further supported by the relative lack of large September snowfall events throughout Colorado's climatology (U.S. Department of Commerce 2024), outside of a few outlier events. Anomalies of variables are computed at each grid point relative to a rolling 21-day average climatology that is centered on each 6-h time step and constructed from the full 42-yr dataset (1980–2021). For times in which hourly cyclone statistics do not match exactly with a 6-h analysis time, we compute anomalies relative to the climatological values associated with the nearest 6-h analysis time. The study region for this analysis is focused on the central United States and the Colorado Front Range since previous work identifies this region as a common genesis location for ETCs (Bentley et al. 2019; Fritzen et al. 2021).

To identify and track central U.S. ETCs, the surface cyclone detection algorithm developed by Wernli and Schwierz (2006), and extended to work with ERA5 data by Sprenger et al. (2017), is used. Surface ETCs are identified when an outermost MSLP contour encloses one or more MSLP minima.

ETC Track

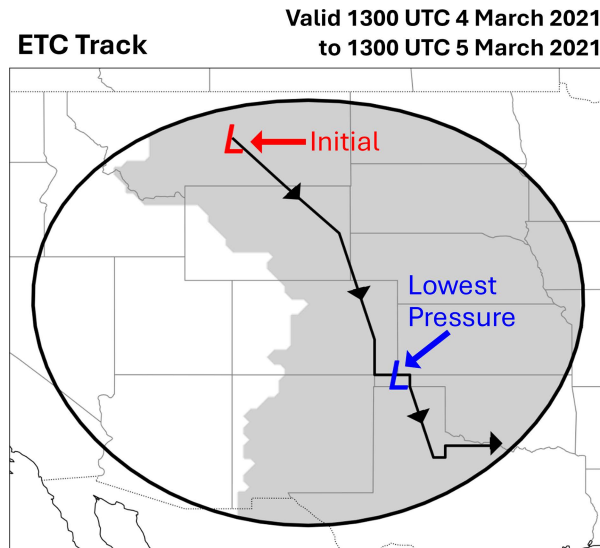**Valid 1300 UTC 4 March 2021 to 1300 UTC 5 March 2021**

FIG. 1. ETC track valid between 1300 UTC 4 Mar 2021 and 1300 UTC 5 Mar 2021. The study domain is shown in gray. The ETC's track is shown using a black line with arrowheads, indicating the direction of ETC movement. The ETC's initial and lowest pressure locations are denoted with red and blue L symbols, respectively.

This algorithm implements terrain filtering, in which ETCs located at elevations above 1500 m are excluded from the dataset. Therefore, the algorithm retains ETCs that develop across lower-elevation regions east of the Continental Divide (i.e., the gray shading in Fig. 1). A radius of 1000 km from central Colorado (39.6339°N, 105.8169°W) is used to define a horizontal boundary for the study domain (i.e., black line in Fig. 1) to capture areas across the central United States that reside east of the Continental Divide between Canada and Mexico. A 1000-km radius is chosen to represent the Rossby radius of deformation for synoptic-scale flow features, which facilitates the identification of ETCs that are likely to induce sensible weather impacts across a large area of the central United States. From there, all ETCs west of the Continental Divide are removed, with the purpose of investigating cyclones that develop, or redevelop, leeward of the Continental Divide. This resulting study domain is pictured by the gray shading in Fig. 1. To prevent results from being biased by cyclones that primarily exist outside of the study domain and only briefly enter the domain, cyclones are required to reside within the study domain for at least 12 h to be considered as part of our dataset.

The first time at which an ETC is identified within the domain, and is in compliance with the aforementioned criteria, is defined as its "initial time." This includes all ETCs that develop, redevelop, and/or enter the domain. ETCs during the cool-season months (October–May) are allowed to persist into subsequent months (e.g., an ETC that undergoes genesis during May is allowed to persist into June). The time at which an ETC exhibits its minimum central MSLP while in the study domain is defined as its "lowest pressure time." If an ETC features more than one time with the same minimum pressure, then the first time featuring that pressure is used. An example ETC track with its initial and lowest pressure locations annotated is shown in Fig. 1. This methodology identified a total of 4723 central U.S. ETCs that form the basis of the analyses performed throughout this study.

3. Lee cyclone statistics

The annual frequency and lowest pressure trends for central U.S. lee cyclones are provided in Fig. 2 for the 1980–2021 cool season (October–May). While annual ETC activity has significantly increased at the 99% confidence interval ($r = 0.66$, $p = 0.00$) from roughly 100 ETCs per year in 1980 to 120 ETCs per year in 2021, the average minimum central pressure of ETCs did not significantly increase and instead hovered around 1002 hPa ($r = 0.19$, $p = 0.22$) across the 42-yr period. The
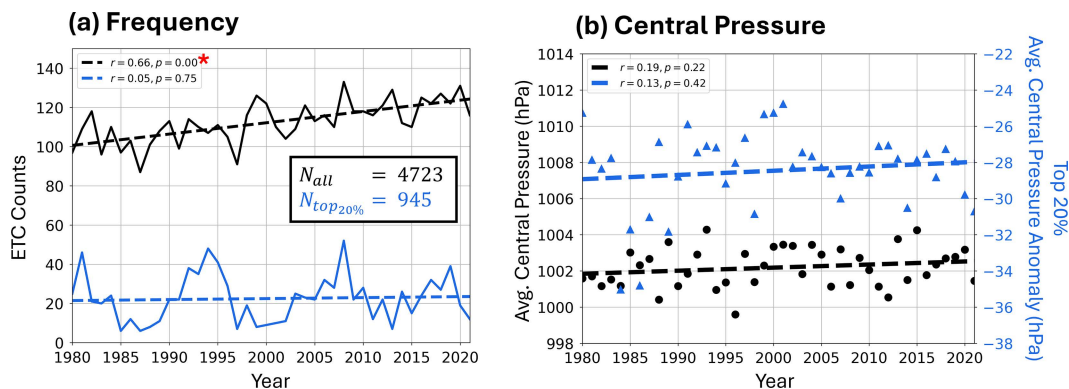

FIG. 2. (a) Annual frequency for all ETCs (black) and the top 20% ETCs (blue) during October–May 1980–2021. (b) Average minimum central pressure for all ETCs (black; hPa) and the average minimum central pressure anomaly for the top 20% ETCs (blue; hPa) during October–May 1980–2021. The dashed contours represent linear regression lines fitted to the (a) annual frequency data and (b) the average minimum central pressure data. Regression correlation coefficients (r) and p values (p) are provided for all trends in the legend. Significant trends at the 95% confidence interval ($p < 0.05$) are marked with a red star.
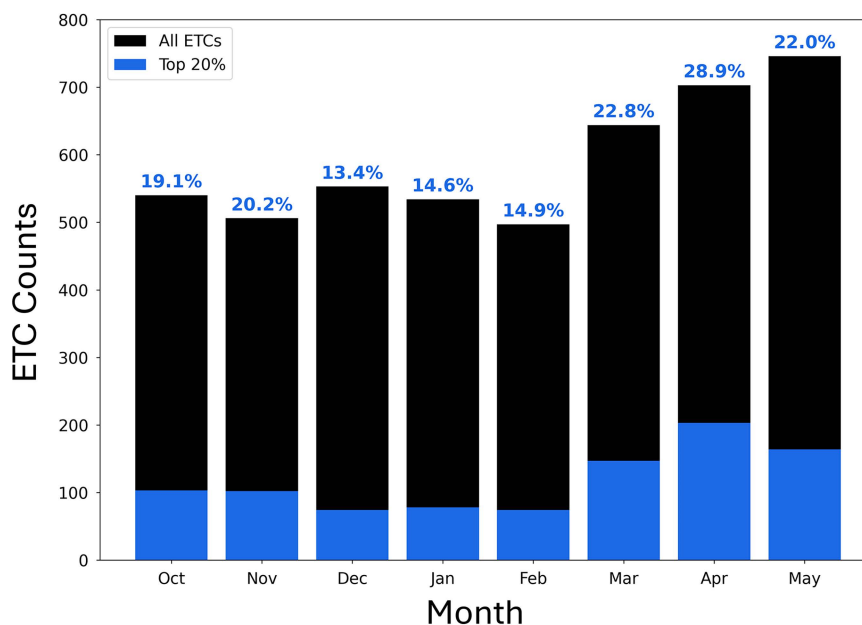
FIG. 3. Monthly ETC frequency (black) and top 20% ETC frequency (blue). The percentages of ETCs in each month that are top 20% ETCs are denoted in blue text at the top of each month's bar.

frequency trend for ETCs that rank in the top 20th percentile in terms of the magnitude of their MSLP anomalies is denoted by the blue line in Fig. 2a. These ETCs feature the most anomalous ETC minimum central pressures and will henceforward be referred to as the "top 20%" subset of ETCs in this study. This suite of anomalous ETCs exhibits an insignificant frequency trend over the climatological period ($r = 0.05$, $p = 0.75$), with an average of nearly 20 top 20% ETCs per year. The lack of a trend is likely related to the strong interannual variability that characterizes this subset, in which some years have as many as 40 top 20% ETCs, and other years have fewer than 10 top 20% ETCs. Likewise, the average minimum central pressure anomalies for the top 20% ETCs exhibit no significant trend ($r = 0.13$, $p = 0.42$) and are typically on the order from −26 to −30 hPa below the climatological mean. The results from Fig. 2 demonstrate that while ETCs are increasing in frequency across the central United States, the most anomalous ETCs are not becoming more frequent.

Most ETCs form during May, April, and March (spring), respectively, while the fewest ETCs occur during February and November, respectively (Fig. 3). While April has the second highest number of ETCs, it features the highest percentage of top 20% ETCs (28.9%) for any month, with March and May close behind (22.8% and 22.0%, respectively). December contains the fewest top 20% ETCs (13.4%). To further explore ETC seasonality, Fig. 4 shows the seasonal partition of ETC frequency and pressure trends over the study period. Figure 4 demonstrates that the total ETC frequency trend observed in Fig. 2 can be attributed to the spring and winter seasons (Figs. 4b,c), with an average increase from nearly 45 ETCs to 55 ETCs ($r = 0.57$, $p = 0.00$) in spring and an increase from

35 ETCs to over 40 ETCs ($r = 0.40$, $p = 0.01$) in winter. No statistically significant trend in ETC frequency is observed during the fall (Fig. 4a). Similar to the full climatology, the seasonal minimum central pressure trends are insignificant. There is a more notable negative trend in the minimum central pressure anomalies for top 20% ETCs during the fall (Fig. 4d), but this trend is not significant. Top 20% ETCs consistently feature the most anomalous average minimum central pressure anomalies during spring, with pressure anomalies near −25 hPa. Since minimum central pressure anomaly trends are insignificant, no inferences can be made about whether stronger ETCs are becoming more frequent on a seasonal basis over the 42-yr climatological period.

Spatially, ETCs (Fig. 5a) are focused closest to the Continental Divide at their lowest pressure time, implying the importance of orographic effects for inducing lee cyclogenesis in this region. A broad cluster of grid points with high ETC counts stretches across the eastern border of Colorado, the Oklahoma Panhandle, northern Texas, and eastern New Mexico. This is consistent with prior work that highlights this region as a location in which Colorado lows are most likely to form (Bentley et al. 2019; Fritzen et al. 2021). Similarly, there are grid points with high ETC counts near the Wyoming/Montana border, consistent with where Bighorn lows frequently develop in the lee of the Rocky Mountains (Fritzen et al. 2021). Bighorn lows follow a similar storm track as Colorado lows, often traveling eastward toward the Great Lakes region. These two areas of lee cyclogenesis are exceptionally prominent when considering the spatial distribution of the top 20% ETCs (Fig. 5b). One notable difference, however, is that top 20% ETCs corresponding to Colorado lows are more isolated near
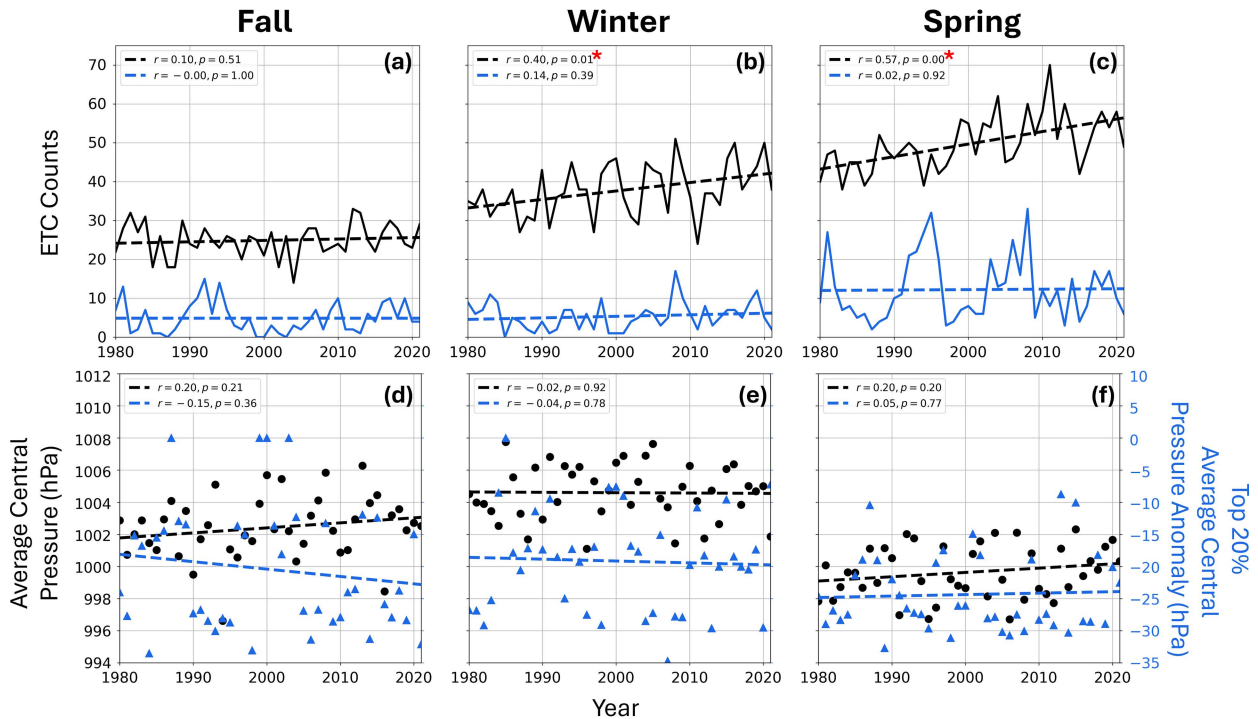
FIG. 4. As in Fig. 2, but parsed by season. Fall includes October and November ($N = 1046$, $N_{\text{top20\%}} = 205$); winter includes December, January, and February ($N = 1584$, $N_{\text{top20\%}} = 226$); and spring includes March, April, and May ($N = 2093$, $N_{\text{top20\%}} = 514$).

the southeastern border of Colorado compared to all ETCs. Transitioning from fall through spring, the frequency of ETCs at their lowest pressure time increases farther east of the Continental Divide, as shown in Figs. 6a–c. This result is likely a function of the larger number of ETCs that occur in the spring compared to fall and winter (Fig. 4). This same pattern is also evident for the top 20% ETCs (Figs. 6d–f). The regional dominance of Bighorn lows and Colorado lows is especially evident in the seasonal spatial locations of the top 20% ETCs (Figs. 6d–f), with two distinct ETC frequency maxima near northern Wyoming and eastern Colorado, respectively, for each season.

4. Variability in cyclone characteristics

a. Self-organizing map algorithm

The self-organizing map (SOM) algorithm is an unsupervised neural network method that groups data based on spatial patterns into clusters known as nodes (Kohonen 2001). The SOM method is chosen for this study due to its ability to effectively ingest high-dimensional data and distill that data into a set of distinct patterns that describe the complex variability of central U.S. lee cyclones. For a detailed description of the SOM algorithm, see Cassano et al. (2015) and Baiman et al. (2023).
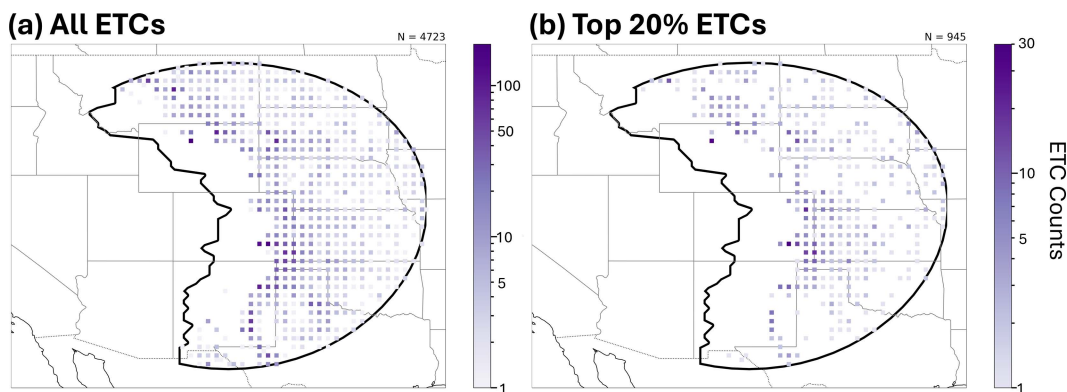

FIG. 5. The location of ETCs at their lowest pressure time during October–May 1980–2021 for (a) all ETCs and (b) top 20% ETCs. Note that a different logarithmic scale is used for each subplot.
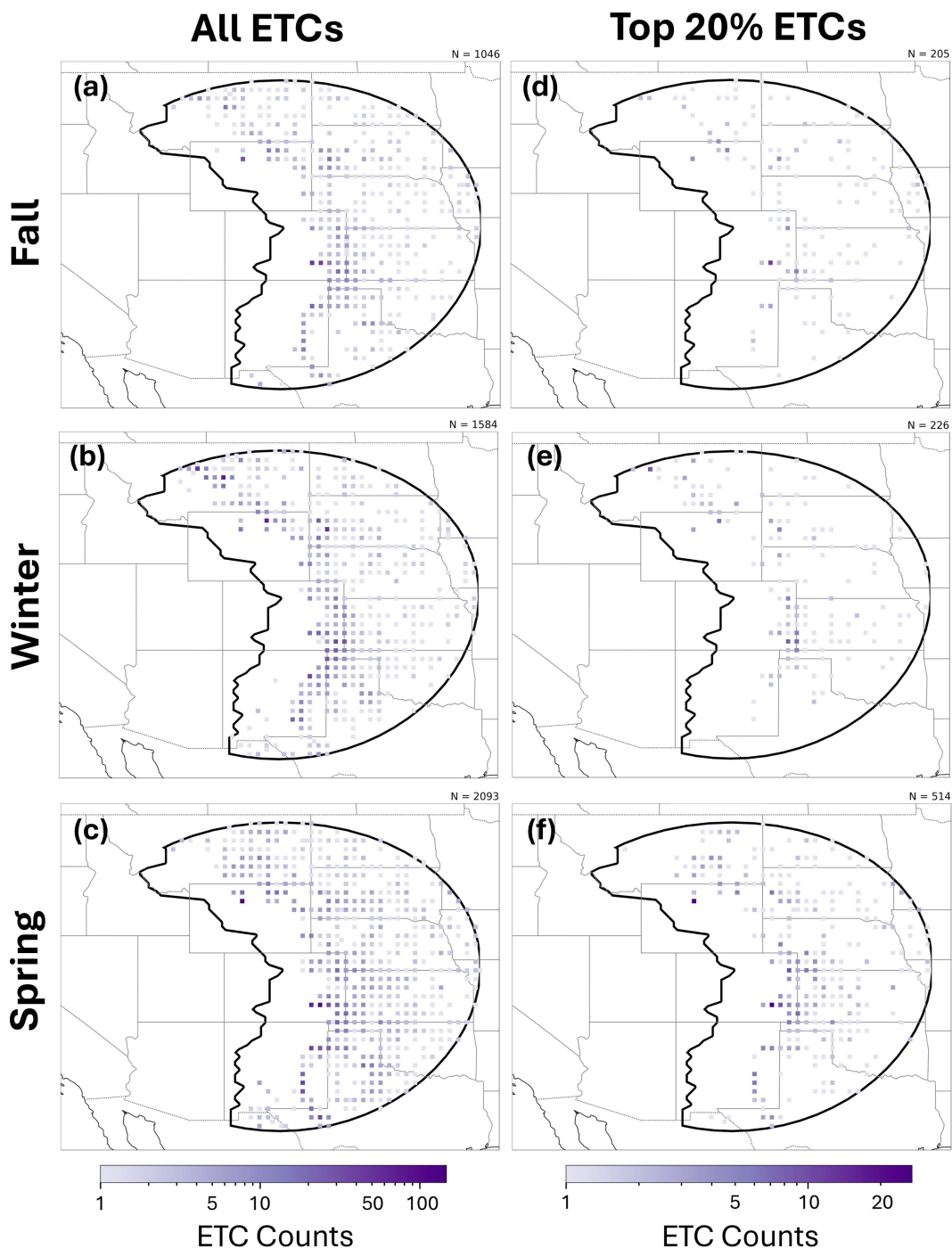
FIG. 6. As in Fig. 5, but parsed by season.

The resultant SOM (Fig. 7) was trained using ERA5 MSLP anomalies east of the Continental Divide during each ETC's lowest pressure time. The SOM shows different ETCs grouped by location and MSLP anomaly intensity. The left-most column and bottom row of the SOM feature the stronger ETCs in terms of MSLP anomalies, whereas moving to the top-right corner of the SOM highlights the weaker ETCs. Spatial

frequency maps and information about ETC lifespan and track length for each SOM node can be found in Figs. S1 and S2 and Table S1, respectively, in the online supplemental material. Gaussian smoothing with a degree of 25 is applied to all variables after compositing to reduce noise due to the complex topography for Fig. 7 and the remaining SOM composite figures in this study. A variety of SOM shapes, sizes,
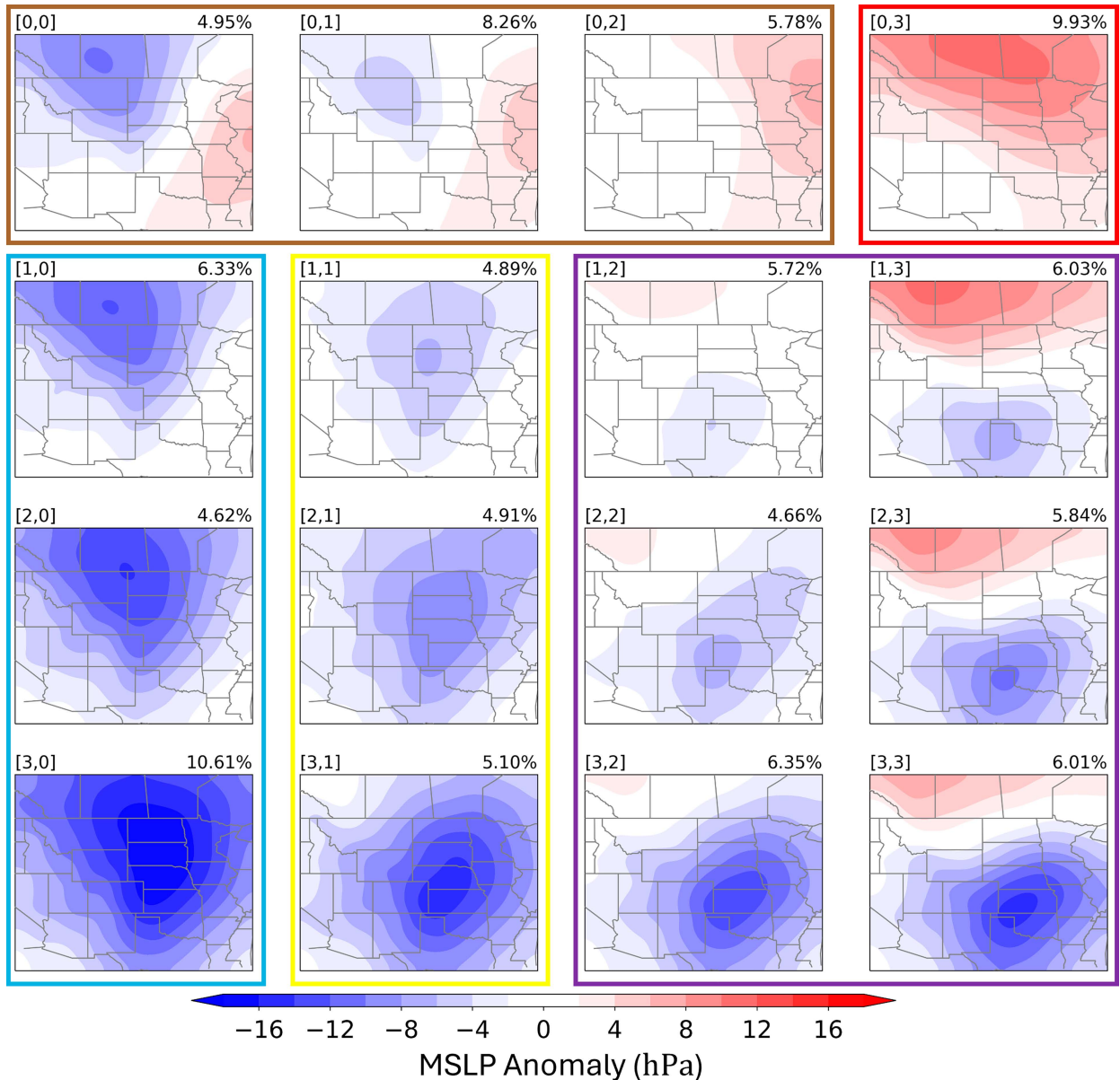
FIG. 7. SOM of MSLP anomalies (shading; hPa). Each SOM node is labeled from [0, 0] to [3, 3] at the top left along with the overall frequency of that node at the top right (percentage of ETCs in a given node out of all $N = 4723$ ETCs). The five SOM clusters are outlined in colored boxes: 1) Mississippi River Valley anticyclone in brown, 2) Canadian anticyclone in red, 3) Northern Plains cyclone in light blue, 4) Central Plains cyclone in yellow, and 5) Southern Plains cyclone in purple.

and learning parameters were tested to produce a robust SOM that highlights unique characteristics of central U.S. ETCs. A 4 × 4 SOM (16 nodes) that uses rectangular topology, the bubble neighborhood function, and Euclidean distance, as described in Kohonen (1982), was used for this study. This SOM exhibited a flat Sammon map topology (Fig. S3; Sammon 1969) and a median Pearson's correlation coefficient of 0.73 (Fig. S4), indicating that the SOM is a good representation of ETC variability. The resultant 16 nodes are further sorted subjectively into five clusters based on their distinctive MSLP anomaly patterns.

The Mississippi River Valley anticyclone cluster (brown outline in Fig. 7; nodes [0, 0], [0, 1], and [0, 2]) features an anticyclone over the Mississippi River Valley and neutral-to-negative MSLP anomalies near the Canadian border and across the western United States. The normalized average ETC tracks for this cluster (Fig. 8a) feature initial locations across Wyoming and shorter track lengths compared to other clusters due to this cluster containing some of the weaker ETCs out of the SOM. The top 20% ETC tracks (Fig. 8b) exhibit initial locations in Wyoming and Montana and farther eastward propagation compared to all ETC tracks for this cluster. This cluster represents
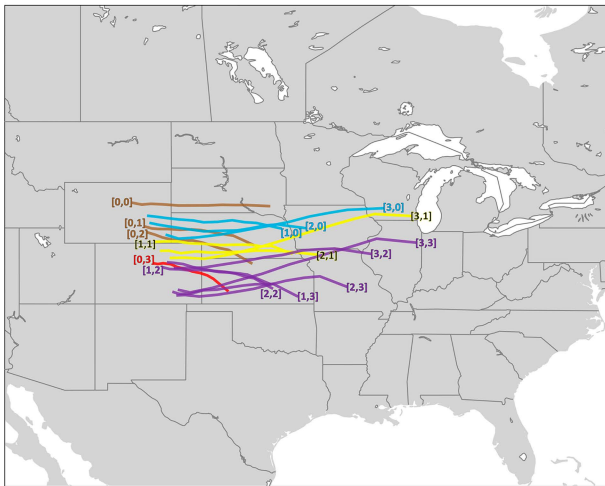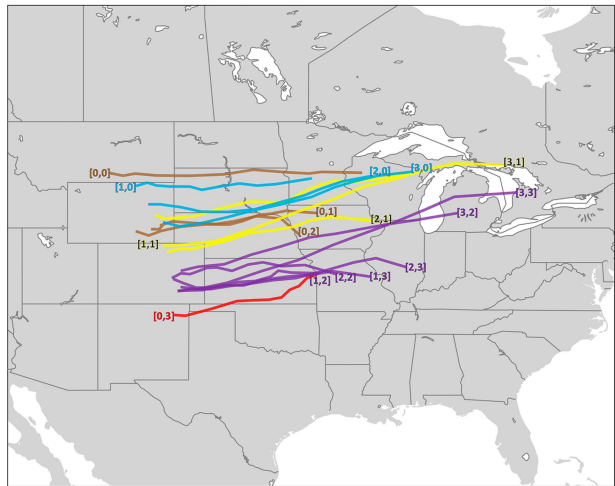
(a) All ETCs

(b) Top 20% ETCs

FIG. 8. Normalized average ETC storm tracks for each SOM node (labels) for (a) all ETCs and (b) top 20% ETCs. To calculate the normalized average ETC tracks, the position of each ETC at every 10% temporal interval of its lifespan is saved and then averaged across all ETCs in each SOM node. Tracks are colored by clusters as in Fig. 7.

18.99% of all central U.S. ETCs. When examining the annual average frequency of the three nodes that comprise the Mississippi River Valley anticyclone cluster in Fig. 9, no significant trends are found for all ETCs or the top 20% ETCs included in the cluster. Each of the three nodes in this cluster experienced fewer than five top 20% ETCs per year, on average, with these highly anomalous ETCs occurring most often during March, April, and May (Fig. 10).

The Canadian anticyclone cluster (red outline in Fig. 7; node [0, 3]) features a dominant surface anticyclone near the Canadian border and neutral MSLP anomalies over the southwestern United States. This cluster represents 9.93% of central U.S. ETCs. The normalized average ETC track for this cluster (Fig. 8a) features an initial location in Colorado and the shortest track length compared to all SOM nodes, likely related to this cluster featuring the weakest ETCs. The top 20% ETC track (Fig. 8b) shows an initial location farther southward in northeast New Mexico and a track that travels northeastward, as opposed to the southeastward propagation implied for all ETCs within this cluster. On average, the Canadian anticyclone cluster has been significantly increasing in frequency over the 42-yr period of study (Fig. 9; $r = 0.43$, $p < 0.05$), but there are only a small number of top 20% ETCs associated with this node that primarily occur during March, April, and May (Fig. 10). Overall, this node is most frequent during December, January, and March, respectively.

The Northern Plains cyclone cluster (light blue outline in Fig. 7; nodes [1, 0], [2, 0], and [3, 0]) features strong negative MSLP anomalies that are focused near the U.S./Canadian border and extend southward into the Central Plains. The normalized average ETC tracks for this cluster (Fig. 8a) start across Wyoming and propagate east/northeastward. The top 20% ETC tracks (Fig. 8b) also start in Wyoming, with tracks [2, 0] and [3, 0] extending farther eastward toward the Great Lakes region compared to [1, 0], likely due to the increased

intensity and thus the lifespan of these nodes. The three nodes in this cluster represent 21.56% of all ETCs, with node [3, 0] containing the largest number of ETCs compared to all nodes. There are no significant annual trends in ETCs or top 20% ETC frequency over the study period for this cluster (Fig. 9), but node [3, 0] exhibits substantial interannual variability for all ETCs and top 20% ETCs. Node [1, 0], which features the weakest MSLP anomalies near the Canadian border compared to the other nodes in the cluster, exhibits the most ETCs ($N = 70$) and top 20% ETCs ($N = 15$) during May (Fig. 10). Conversely, node [3, 0] has fewer than 40 ETCs during May, but nearly half of these are top 20% ETCs. Node [3, 0] is characterized by a dominant surface cyclone that extends from Canada to Colorado/Kansas and features the largest MSLP anomalies compared to all nodes (Fig. 7), justifying why this node is associated with the most top 20% ETCs when parsed by both year and month.

Nodes that exhibit negative MSLP anomalies that are centered farther south than the Northern Plains cyclone cluster correspond to the Central Plains cyclone cluster (yellow outline in Fig. 7; nodes [1, 1], [2, 1], and [3, 1]). The normalized average ETC tracks for this cluster (Fig. 8a) start across Wyoming and northeast Colorado. The top 20% ETC tracks (Fig. 8b) also show initial locations in Wyoming and Colorado, with track [3, 1] extending farther eastward into the Great Lakes region compared to nodes [2, 1] and [1, 1]. The Central Plains cyclone cluster contains 14.90% of all ETCs. As the MSLP gradient and magnitude of negative MSLP anomalies increase moving toward the bottom of the SOM (from [1, 1] to [3, 1]) in this cluster, more top 20% ETCs are observed per node (Fig. 9). However, the frequency of all ETCs is consistently close to five ETCs per year for each node. There are no significant trends in annual ETC frequency over the study period for any node in this cluster. Also, ETC frequency during the shoulder months (October, April, and May) is higher for
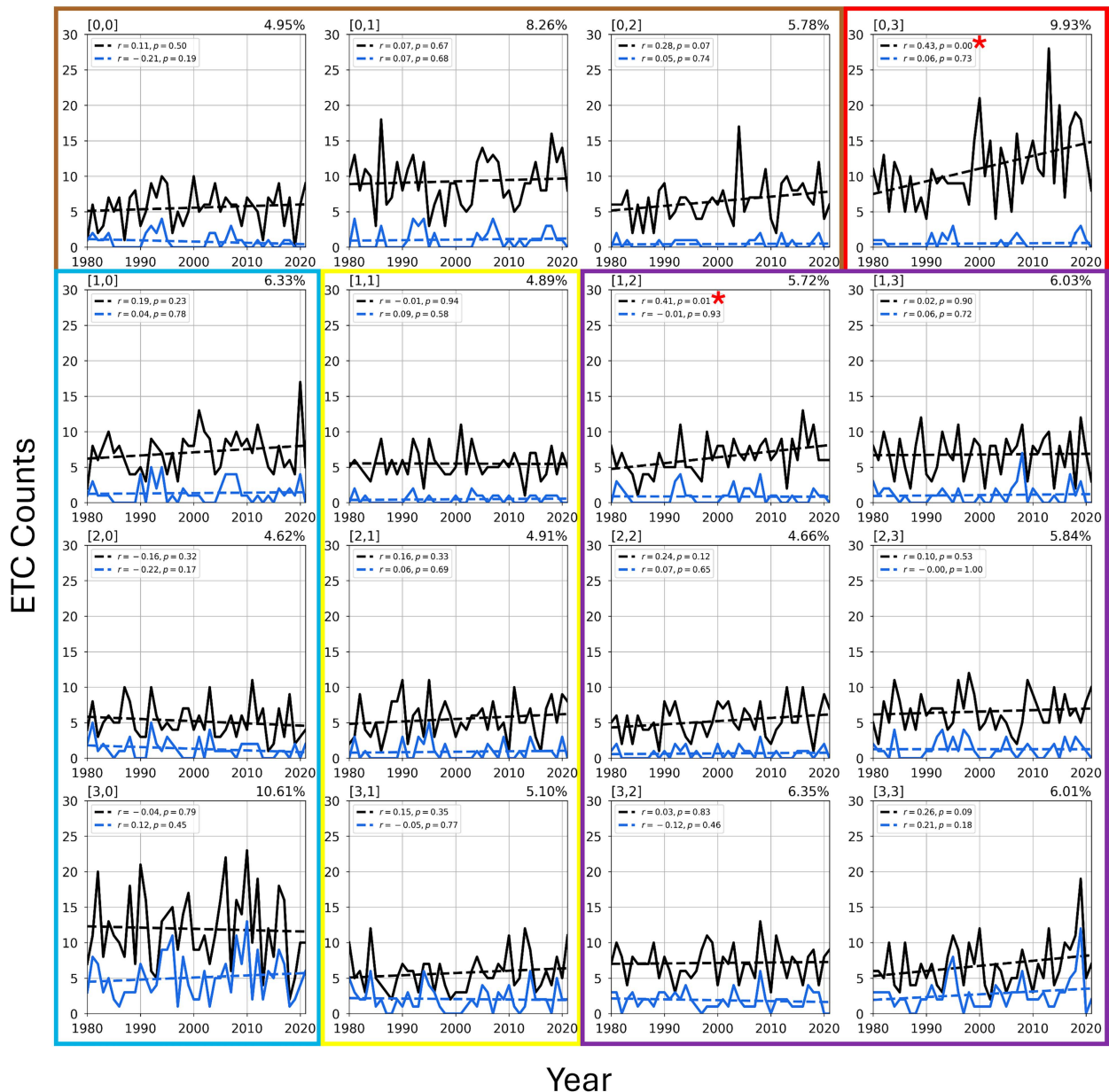
FIG. 9. As in Fig. 2a, but parsed by SOM node. SOM clusters are outlined with colored boxes as in Fig. 7.

nodes that exhibit weaker MSLP anomalies in this cluster (i.e., nodes [1, 1] and [2, 1]; Fig. 10).

The final SOM cluster is the Southern Plains cyclone cluster (purple outline in Fig. 7; nodes [1, 2], [1, 3], [2, 2], [2, 3], [3, 2], and [3, 3]). This cluster features a north–south high–low pressure anomaly dipole that increases in intensity when moving toward the bottom-right portion of the SOM (node [3, 3]). The normalized average ETC and top 20% ETC tracks for this cluster (Fig. 8) start across Colorado and propagate to the east/northeast across the central Mississippi River Valley and southern Great Lakes. Nodes [3, 3] and [3, 2] feature some of the longest ETC track lengths throughout the SOM, likely because the ETCs associated with these nodes have stronger

MSLP anomalies and a longer lifespan (Table S1). As the largest SOM cluster featuring six SOM nodes, this cluster comprises 34.61% of all ETCs. The weakest pressure dipole (node [1, 2]) is the only node within the cluster that exhibits a significant increase in annual ETC frequency during 1980–2021 (Fig. 9; $r = 0.41$, $p < 0.05$) and is most often observed during May (Fig. 10). All six nodes display considerable interannual variability in the frequency of all ETCs and top 20% ETCs. Five of the six nodes feature the greatest frequency of top 20% ETCs during April, and for all ETCs, nodes [2, 3] and [3, 3] are generally likely to occur during any month of the study period.

The bottom row of the SOM (nodes [3, 0], [3, 1], [3, 2], and [3, 3]) represents a collection of nodes that feature the
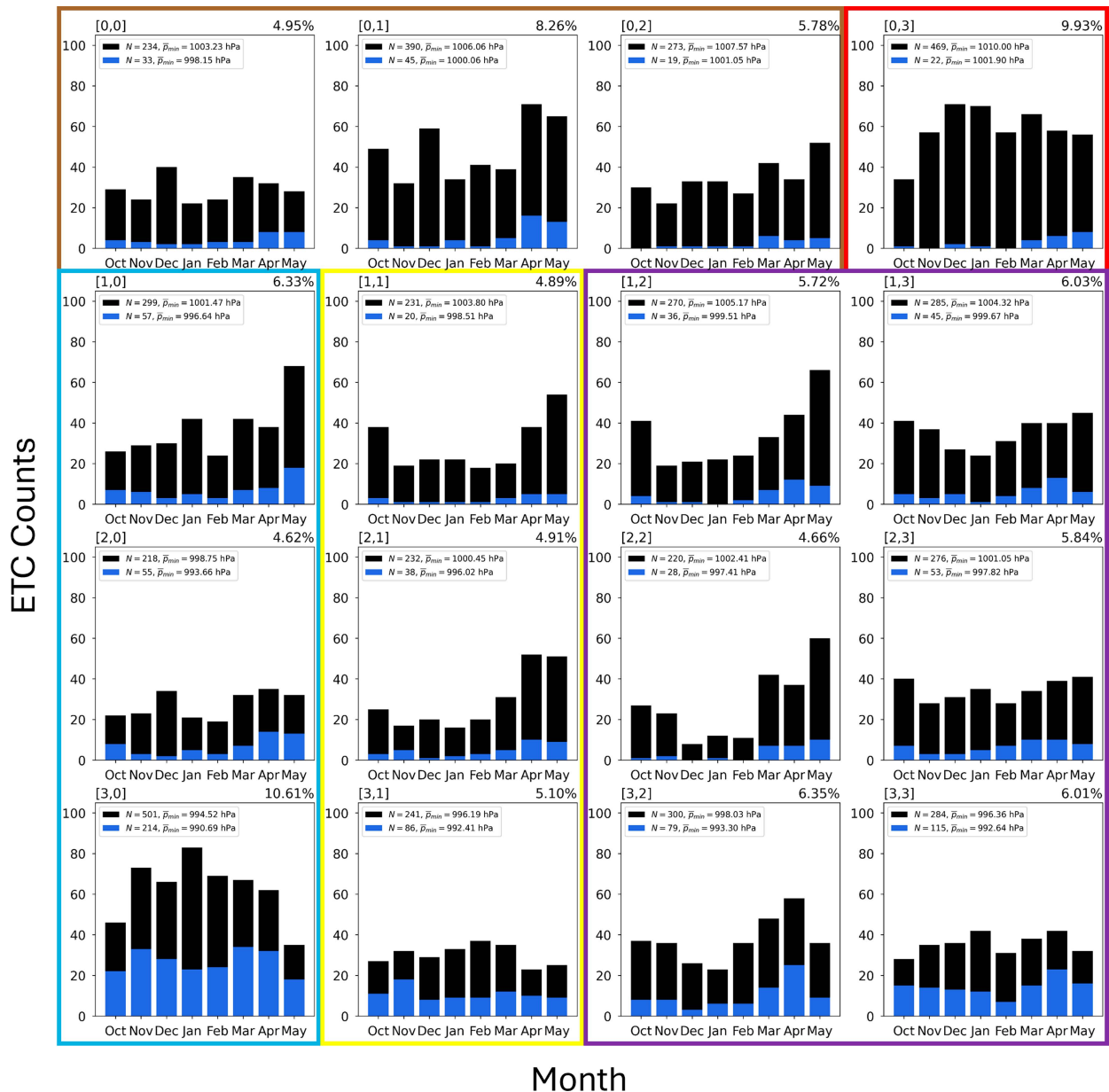
FIG. 10. As in Fig. 3, but parsed by SOM node. The number of ETCs, top 20% ETCs, and average minimum central pressure for each category of ETCs are shown in the legend for each node. SOM clusters are outlined with colored boxes as in Fig. 7.

most top 20% ETCs, indicating that these synoptic environments with widespread negative MSLP anomalies are particularly conducive to producing strong ETCs across the central United States.

b. Upper-level environments and dynamics

After categorizing the 16 SOM nodes into five clusters, composite upper-level flow patterns were constructed for the ETCs mapping to each node to identify differences between the upper-level dynamics associated with each cluster. To investigate ETC impacts regardless of their geographical location, ETC-centered composites are developed. In particular, a

60° latitude by 120° longitude box centered on the location of minimum pressure was isolated for each ETC. Data within the box were then extracted for each ETC and weighted based on the cosine of latitude. The data were then summed together across all times and divided by the sum of the latitudinal weights. This methodology results in an ETC-centered composite that displays the average distribution of a chosen variable in the vicinity of each type of central U.S. ETC. This compositing technique is used in this study to investigate upper- and lower-level dynamics of the ETCs. Note that the forthcoming composites are plotted against a geographic map background based on the average ETC center location for
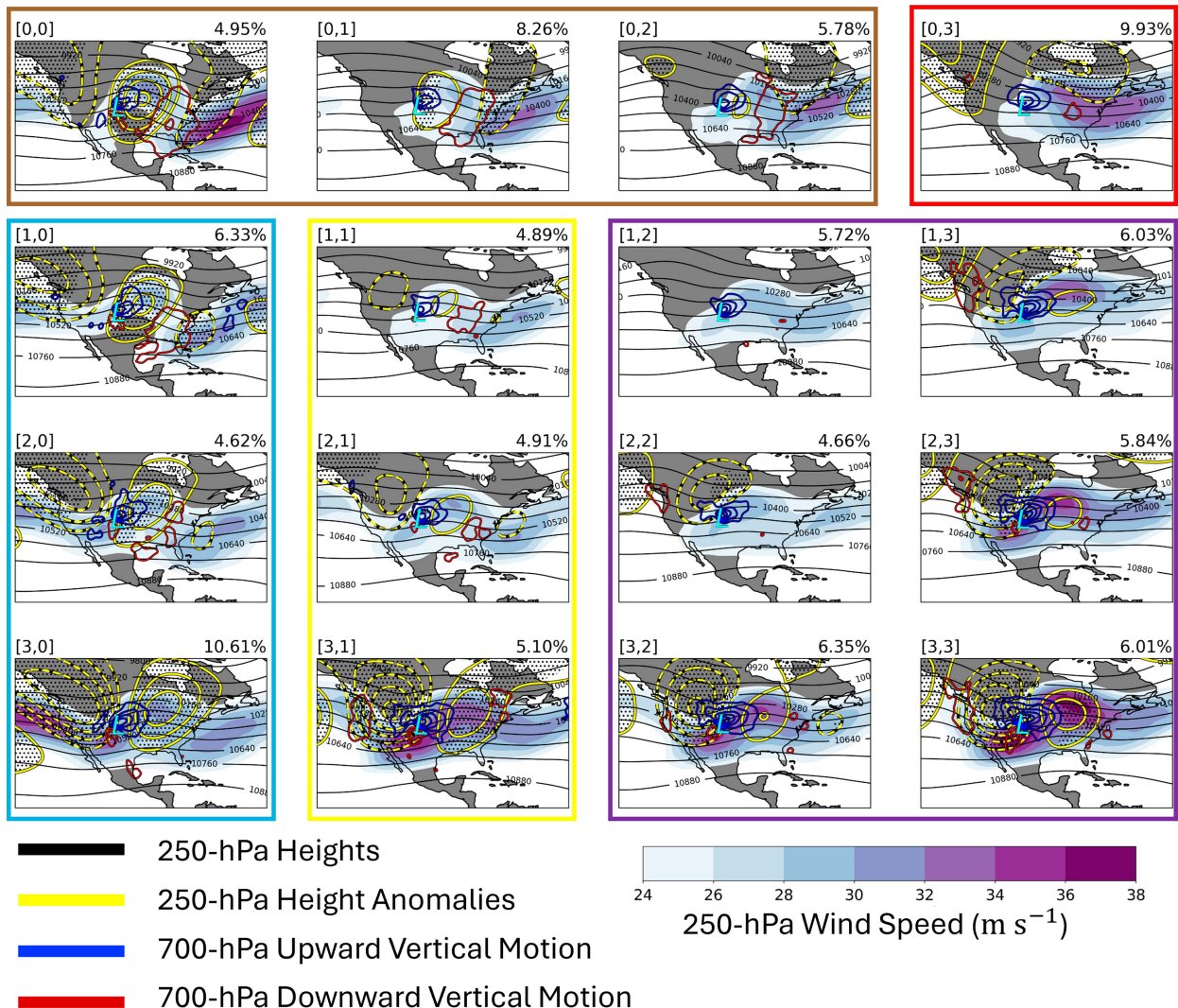
FIG. 11. ETC-centered composites at the lowest pressure time of the upper-tropospheric flow pattern for ETC events associated with each SOM node, with 250-hPa geopotential height (solid black lines, contoured every 120 m), 250-hPa geopotential height anomalies (contoured every 30 m in solid yellow where positive and in dashed yellow where negative), 250-hPa wind speed (shaded according to the fill pattern; m s^{-1}), and 700-hPa vertical motion (contoured every 0.5 dPa s^{-1} in blue for ascent and red for descent). The average ETC center per node is denoted with a cyan L symbol. Stippling indicates where the 250-hPa geopotential height anomalies are significant at the 99% confidence interval based on a bootstrap resampling test in which 1000 random composites were generated using the full collection of central U.S. ETC time steps. SOM clusters are outlined with colored boxes as in Fig. 7. Plotted variables are smoothed following the methodology in Fig. 7.

each SOM node to provide geographic context for the average location of the ETC at its lowest pressure time.

The Mississippi River Valley anticyclone cluster (Fig. 11) features a strong jet streak that extends over the U.S. East Coast and the western North Atlantic. Over the central United States, the jet features weaker composite wind speeds compared to the downstream jet streak over the North Atlantic. All three nodes show a shortwave trough to the west of the Continental Divide and a region of positive height anomalies over the Mississippi River Valley. A region of enhanced 700-hPa ascent is located beneath the right-entrance region of the jet streak over central Canada. Conversely, a broad

region of descent is observed beneath the left-entrance region of the stronger jet streak over the eastern United States. Node [0, 0] exhibits the strongest vertical motion across all three nodes in the cluster due to the enhanced upper-level flow curvature and stronger jet streaks accompanying that node.

Similar to the Mississippi River Valley anticyclone cluster, the Canadian anticyclone cluster (Fig. 11) features a strong jet streak over the U.S. East Coast, but with a more zonal orientation. Average peak jet streak wind speeds are around 32 m s^{-1} and centered on the U.S. mid-Atlantic coast. An upper-level ridge is positioned over the U.S. West Coast,

collocated with a large region of positive geopotential height anomalies. Descent is present beneath the entrance region of the aforementioned jet streak, helping to foster the development of the dominant surface anticyclone near the Canadian border downstream of the western North American ridge.

The North Pacific jet is a comparatively more notable jet streak feature for all nodes within the Northern Plains cyclone cluster (Fig. 11). Moving down the SOM from node [1, 0] to [3, 0], the North Pacific jet increases in intensity and is associated with a progressively more amplified trough over the western United States. The north-central United States is located east of the trough axis and beneath the left-exit region of the extended North Pacific jet, which favors ascent over the region. This ascent is further enhanced by the entrance region of an additional jet streak farther downstream over the north-central United States. We hypothesize that ETCs are likely more frequent during winter in node [3, 0] when compared to spring in nodes [1, 0] and [2, 0] because of the strong North Pacific jet stream wind speeds (Fig. 11) that are more common in winter months. A strong signal for downslope flow is also present in all three nodes near the Rocky Mountains, but is especially amplified in node [3, 0].

The North Pacific jet is also somewhat amplified for events within the Central Plains cyclone cluster (Fig. 11), but not as much in comparison to the Northern Plains cyclone cluster. Node [1, 1] features a weak negative MSLP anomaly over most of the study domain (Fig. 7), so it is not surprising that this node has the weakest region of ascent across the central United States when compared to the other nodes within the cluster. Node [2, 1] features two distinct coupled jet streaks to the north and south of the study region, respectively, that facilitate ascent over the central United States. Finally, node [3, 1] highlights a more dynamic environment for ETC development due to the presence of a deeper trough over the western United States and a jet streak located at the base of the trough. The combined upper-level divergence induced by the aforementioned features facilitates a broad region of ascent across the central United States. Paired with the strong signal for downslope flow across the southern Rocky Mountains, node [3, 1] represents one of the most potent dynamical environments within the SOM for lee cyclogenesis.

The six nodes associated with the Southern Plains cyclone cluster (Fig. 11) generally exhibit a coupled jet structure, with one jet streak located near the U.S./Mexico border and an additional jet streak farther poleward over the northern United States. This cluster is defined by the presence of a north–south high–low MSLP anomaly dipole (Fig. 7), with the trough–ridge pattern over the western and eastern United States, respectively, and the jet streak configuration associated with this cluster providing a synoptic-scale environment conducive to surface cyclogenesis and anticyclogenesis across central North America. In particular, the central United States is located east of the trough axis, beneath the southern jet streak's left-exit region, and beneath the northern jet streak's right-entrance region, substantially increasing the magnitude of ascent observed compared to the other nodes and clusters, especially for node [3, 3]. Only nodes [2, 3], [3, 2], and [3, 3] exhibit a signal for strong downslope flow in the lee of the Rocky

Mountains, likely due to the stronger cross-barrier upper-level flow in those three nodes compared to the other three nodes in the cluster. Additionally, the location of the left-entrance region of the northern jet streak supports the development of the stronger anticyclone observed across southern Canada in nodes [1, 3], [2, 3], and [3, 3].

The bottom row of the SOM (nodes [3, 0], [3, 1], [3, 2], and [3, 3]), which represents the nodes with the most top 20% ETCs, exhibits some of the strongest regions of ascent over the central United States across the entire SOM. The favorable synoptic-scale environment for cyclogenesis associated with these nodes helps explain why these four SOM nodes produce a majority of the most anomalous ETCs. Additionally, all four nodes in the bottom row of the SOM feature strong downslope flow to the east of the southern Continental Divide, which can further contribute to vortex stretching and cyclogenesis across the region. A discussion of the vertical motion driven by the $\mathbf{Q}_n$ and $\mathbf{Q}_s$ components of the $\mathbf{Q}$-vector form of the quasigeostrophic omega equation has been included in the supplemental text. As shown in Fig. S5, for the majority of the SOM, the strongest upward vertical motion is driven by $\mathbf{Q}_s$, or variations in along-flow curvature that act to reorient the temperature gradient, rather than frontogenesis and frontolysis.

c. Lower-level environments and dynamics

Within the lower troposphere, the Mississippi River Valley anticyclone cluster (Fig. 12) is characterized by areas of 850-hPa warm anomalies over the Northern and Central Plains that are collocated with regions of anomalous moisture. This setup provides a favorable environment for the development of precipitation within areas of localized warm-air advection to the east of the surface cyclone center. The three nodes within this cluster all exhibit dry anomalies over the Mississippi River Valley. These dry anomalies are coincident with the broad synoptic-scale subsidence induced beneath the North Atlantic jet's left-entrance region (Fig. 11).

The dominant region of high pressure associated with the Canadian anticyclone cluster is collocated with an anomalously dry air mass and the equatorward advection of cold air (Fig. 12). The upper-tropospheric flow pattern for this node indicated a region of ascent over the central United States (Fig. 11), but given the weak synoptic-scale dynamics in place, it is no surprise that the average minimum pressure of ETCs in this node is 1010.0 hPa—the highest across all nodes. Nevertheless, the subtle region of anomalous moisture northeast of the cyclone center is still likely to support some weak precipitation in association with the ETCs that characterize this node.

The strong zonal North Pacific jet pattern that characterizes the Northern Plains cyclone cluster facilitates downslope flow in the lee of the Continental Divide that contributes to ETC development in this cluster (Fig. 11). The effects of this downslope flow are also apparent from the strong 850-hPa warm temperature anomalies that extend eastward from the Continental Divide (Fig. 12). The downslope flow and advection of dry air from the Intermountain West also help to explain the lack of anomalous moisture immediately downstream of the orography and equatorward of the cyclone center. Moving
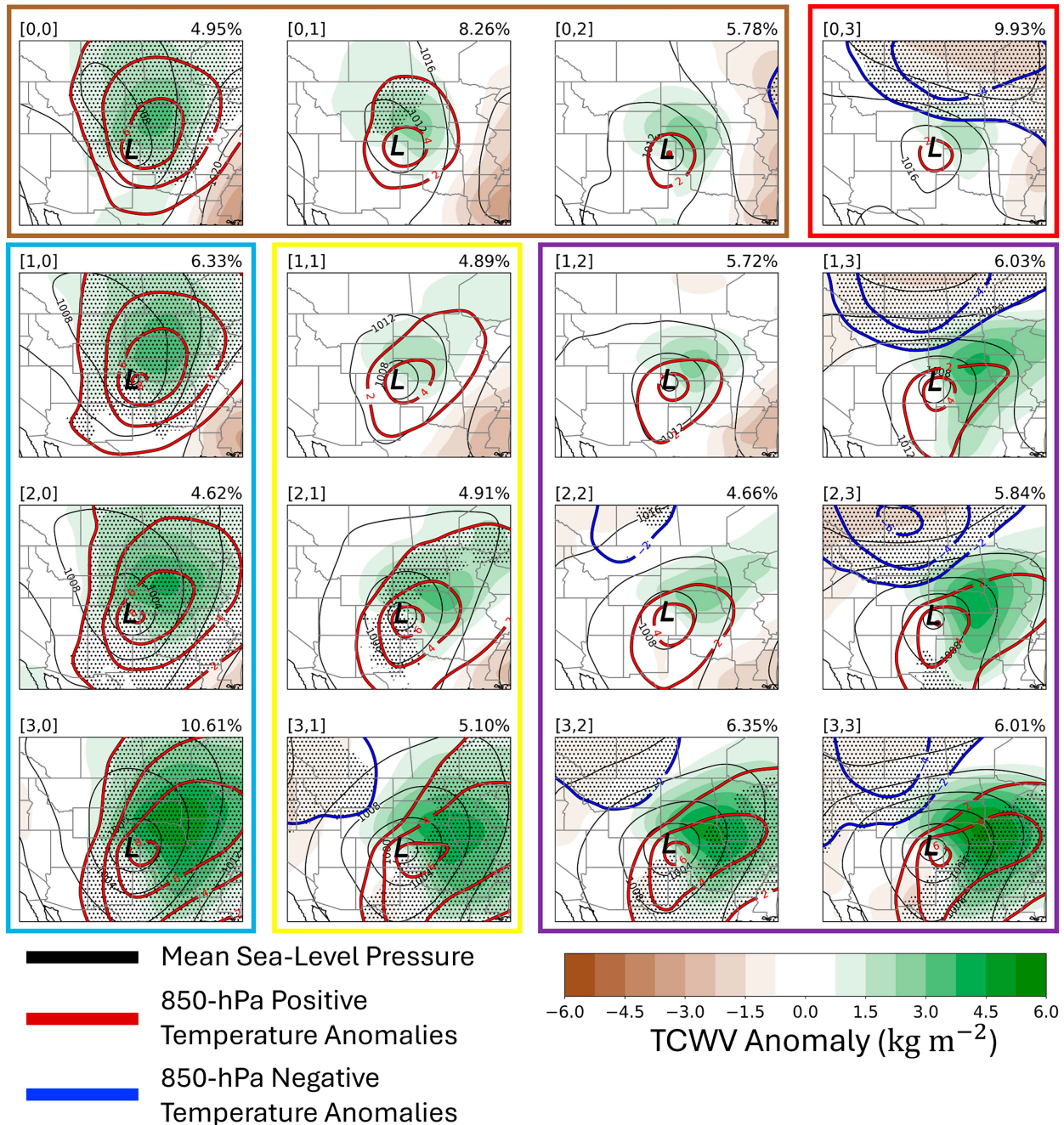
FIG. 12. ETC-centered composites at the lowest pressure time of the lower-tropospheric flow pattern for ETC events associated with each SOM node, with total column water vapor anomalies (shaded according to the fill pattern; kg m^{-2}), 850-hPa temperature anomalies (contoured every 2°C in red where positive and blue where negative), and MSLP (black solid lines; contoured every 4 hPa). The average ETC center per node is denoted with a black L symbol. Stippling indicates where the 850-hPa temperature anomalies are significant at the 99% confidence interval based on a bootstrap resampling test in which 1000 random composites were generated using the full collection of central U.S. ETC time steps. SOM clusters are outlined with colored boxes as in Fig. 7. Plotted variables are smoothed following the methodology in Fig. 7.

down in the SOM from node [1, 0] to node [3, 0], a region of anomalous moisture focused near the U.S./Canadian border increases in magnitude and gradually extends farther south toward Texas and Louisiana. Therefore, node [3, 0], which

features highly anomalous moisture within an area of warm-air advection, is likely to be particularly conducive to wide-spread precipitation production across the western Great Lakes and Mississippi River Valley regions.

A slightly weaker region of warm air anomalies compared to the Northern Plains cluster is observed for the Central Plains cyclone cluster (Fig. 12), with the anomalously warm air mass anchored immediately downstream of the southern Rocky Mountains and extending northeastward across the study domain. The temperature anomalies within this cluster are also focused slightly farther south than those in the Northern Plains cyclone cluster, with the warmest anomalies located southeast of the cyclone center. Anomalous moisture is also collocated with regions characterized by warm-air advection to the northeast of the ETC and generally maximized near areas proximate to and south of the ETC's implied warm front. Node [3, 1] is the only node in the cluster that also features cold air anomalies within the northwestern corner of the domain, highlighting a more baroclinic environment in association with this node. The increased temperature gradient in node [3, 1] to the north of the ETC center acts to focus on robust precipitation production within a region that also features enhanced synoptic-scale ascent induced by an upstream trough and jet streak over the western United States (Fig. 11). We hypothesize that ETCs are likely less frequent during the shoulder seasons in node [3, 1] (Fig. 10) because of the cold air anomalies that characterize the low-level temperature distribution for these nodes northwest of the ETC center and create a stronger baroclinic environment. We believe this temperature anomaly dipole is not present in nodes [1, 1] and [2, 1] because these nodes most frequently occur in the spring when cold Arctic air masses from Canada are less likely to be advected equatorward in conjunction with ETC events. This reduces the temperature contrast in the vicinity of the ETC center than might be typically observed during the winter months.

For the majority of the nodes in the Southern Plains cyclone cluster (Fig. 12), cold-air advection from the north produces a strong anomalous temperature gradient that favors robust ETC development across the Central Plains and Southern Plains. Notably, the anomalous moisture in nodes [3, 2], [3, 3], [2, 3], and [1, 3] is likely sourced from the Gulf of Mexico, providing a favorable thermodynamic environment for the production of precipitation in association with the ETCs in this cluster. Combined with the presence of strong synoptic-scale ascent induced by the prevailing upper-level flow pattern (Fig. 11), ETCs are able to develop within a particularly conducive environment characterized by the presence of exceptional baroclinicity as well as the poleward advection of warm, humid air from the south.

The bottom row of the SOM (nodes [3, 0], [3, 1], [3, 2], and [3, 3]) features some of the most favorable thermodynamic environments across all 16 SOM nodes. Regions of strong warm-air advection in the presence of highly anomalous moisture east of the ETC center are particularly conducive to robust precipitation development. This observation, combined with the fact that these nodes also feature the strongest dynamic forcing for ascent, helps to explain why the most top 20% ETCs are included in these four nodes. It was previously observed that all four of these nodes exhibit strong downslope flow in the lee of the southern Rocky Mountains, which is confirmed by the anomalously strong west–east temperature gradient that extends across the same region. This subsidence, as well as the eastward transport of dry air over the southwestern United States, produces a small region of anomalously dry air south of the ETC center. This warm dry air intrusion (Browning 1997) can play an important role in producing instability near the ETC's implied frontal boundaries.

d. Impacts

To investigate precipitation type and amount, as well as 10-m wind speeds, in the vicinity of central U.S. ETCs, the same cyclone-centered compositing technique used in Figs. 11 and 12 is implemented. One difference, however, is that a smaller 40° latitude × 40° longitude domain centered on the location of minimum pressure is used for each ETC.

At first glance, one notable feature of the Mississippi River Valley anticyclone cluster (Fig. 13) is the preferential displacement of precipitation to the west of the ETC center. Recall that 700-hPa descent (Fig. 11) and an anomalously dry air mass (Fig. 12) are located over the Mississippi River Valley, which likely inhibit the production of robust ETC-related precipitation on the eastern flank of the ETC. Therefore, the majority of precipitation for these nodes (Fig. 13) is focused farther westward, with upslope flow against orography likely contributing to some of the precipitation observed in this sector of the ETC. Additionally, all three nodes feature lower average precipitation totals relative to other SOM nodes because the anomalous region of moisture associated with this precipitation is not as humid as air masses that contribute to precipitation for other nodes of the SOM (i.e., the bottom row of SOM nodes). The appendage of precipitation west of the ETC falls as both rain and snow (Figs. 14 and 15) due to presence of warm temperature anomalies that dominate the region (Fig. 12). A distinct region of faster 10-m winds for this cluster is located within the warm sector to the southeast of the ETC (Fig. 16) where the strongest pressure gradients are found. Compared to other SOM nodes, these wind speeds are weaker than nodes toward the bottom of the SOM, but the locations of these strong wind speeds are comparable to the other nodes. All nodes show greater wind speeds to the southwest of the composite ETC center, which we hypothesize is related to the higher elevation of these locations compared to the rest of the domain.

The precipitation for the Canadian anticyclone cluster (Fig. 13) is primarily positioned north of the ETC and within the warm sector southeast of the ETC. Both locations experience rain, but snow is only observed northwest of the ETC center (Figs. 14 and 15). Compared to other clusters, the lack of a strong baroclinic environment, moisture source, and vigorous synoptic-scale vertical motion all contribute to the weak ETC, lack of substantial precipitation, and relatively weak 10-m wind speeds observed in association with this cluster (Fig. 16). The anomalously dry air mass situated over the northeast portion of the study region (Fig. 12) further inhibits the ETC from producing widespread precipitation compared to other node environments.

Similar to the Mississippi River Valley anticyclone cluster, the Northern Plains cyclone cluster (Fig. 13) also exhibits a
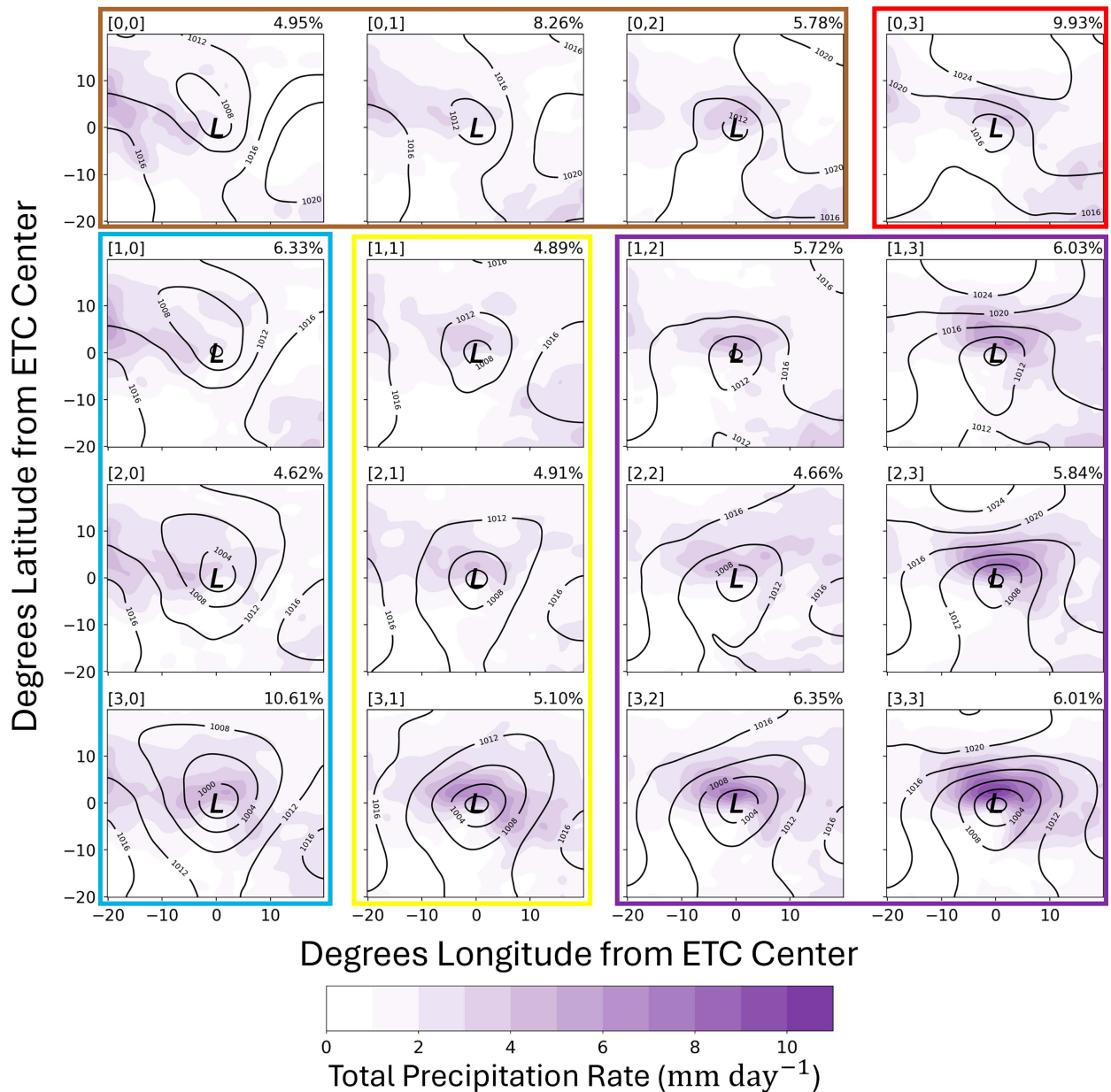
FIG. 13. Average ETC-centered total precipitation rate (purple shading; mm day^{-1}) at the lowest pressure time for each node with MSLP overlaid (black solid lines contoured every 4 hPa). The ETC center is denoted with a black L symbol. SOM clusters are outlined with colored boxes as in Fig. 7. Plotted variables are smoothed following the methodology in Fig. 7.

nonnegligible fraction of the precipitation distribution on the western side of the ETC. This is likely because anomalous moisture is advected westward around the ETC's circulation toward areas of orography west of the ETC (Fig. 12). Node [3, 0] also features precipitation that extends from the western side of the ETC toward the ETC center and into the warm sector. Rain is generally favored in areas closest to the ETC center, where air temperatures are anomalously warm (Fig. 14), and snow is present predominantly to the west and well to the north of the ETC center (Fig. 15). Moving down the SOM from node [1, 0] to [3, 0], precipitation totals (Fig. 13)

and 10-m wind speeds (Fig. 16) near the ETC center generally increase, in line with a more favorable dynamical and thermodynamic environment that accompanies nodes at the bottom of the SOM.

When ETCs are positioned farther south across the central United States in the Central Plains cyclone cluster, precipitation patterns are generally maximized near the ETC center (Fig. 13), with more precipitation coinciding with environments that feature more anomalous moisture and favorable upper-level dynamics (i.e., compare node [1, 1] with [3, 1]). Particularly evident in node [3, 1], rain is the dominant precipitation
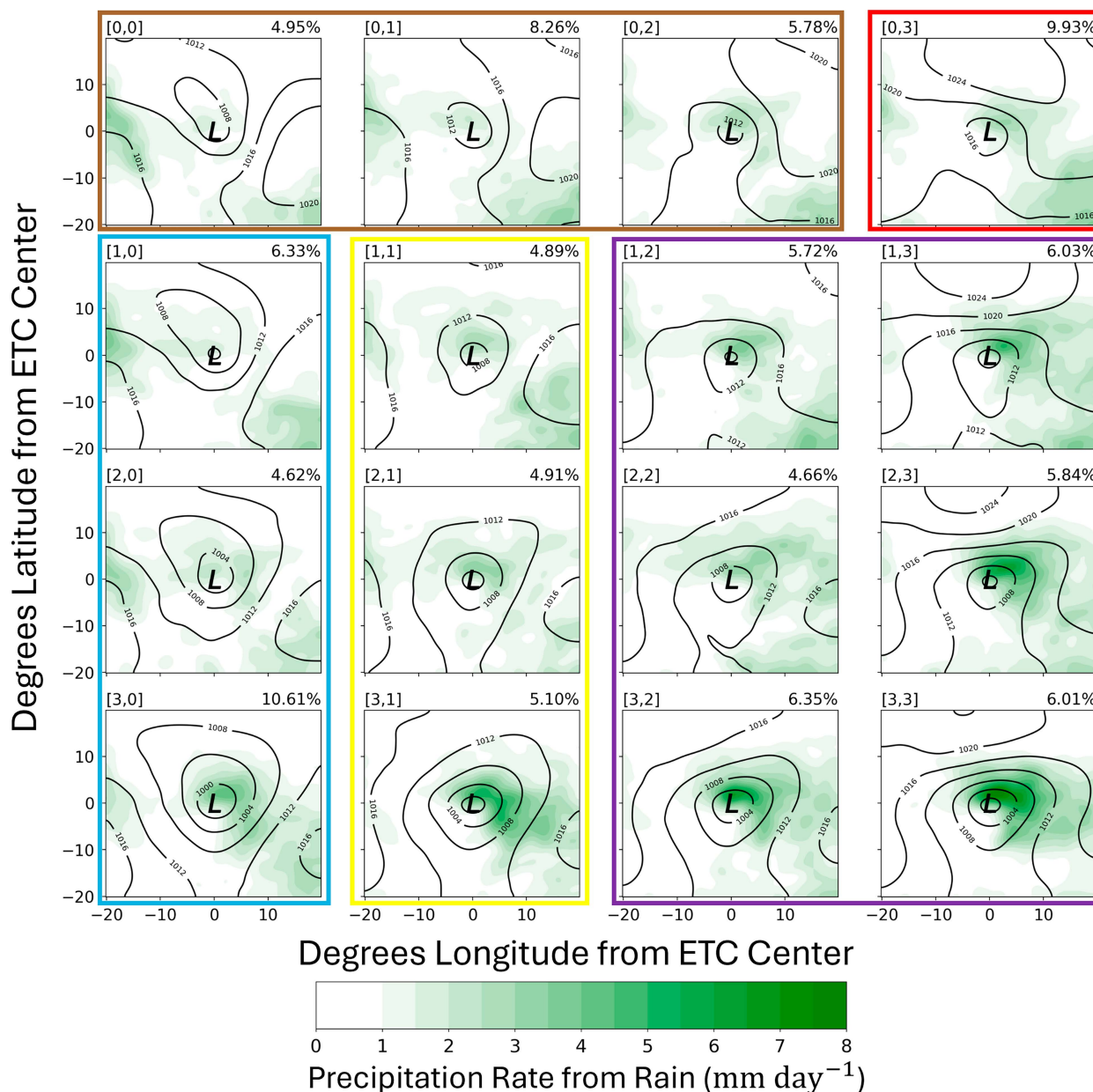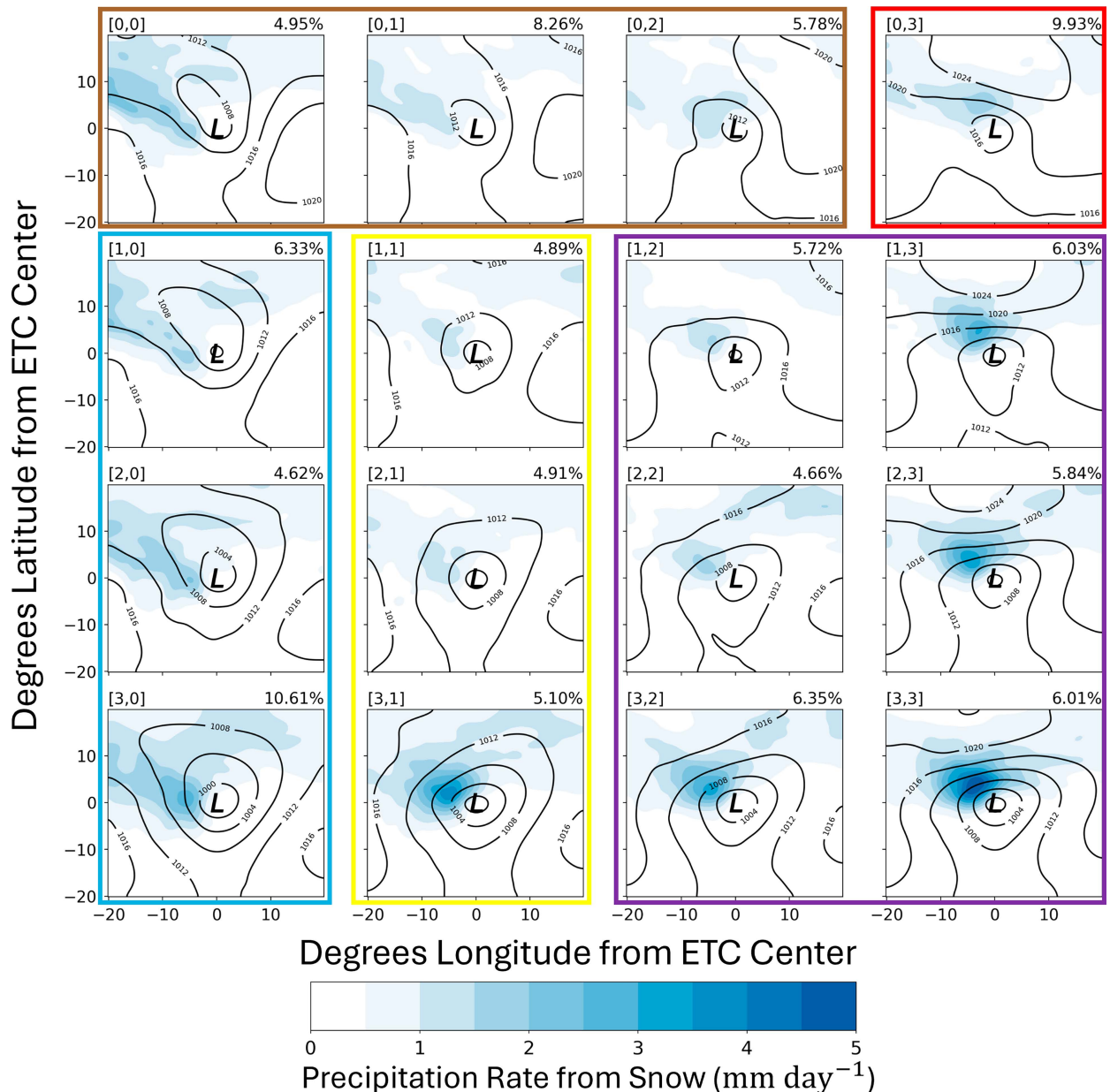
FIG. 14. Average ETC-centered precipitation rate resulting from rain (green shading; mm day^{-1}) at the lowest pressure time for each node, with MSLP overlaid (black solid lines contoured every 4 hPa). The ETC center is denoted with a black L symbol. SOM clusters are outlined with colored boxes as in Fig. 7. Plotted variables are smoothed following the methodology in Fig. 7.

type along the ETC's implied warm front (Fig. 14), whereas snow is the dominant precipitation type west of the ETC center (Fig. 15). Node [3, 1] experiences increased precipitation totals and more separable precipitation types compared to the other two nodes in this cluster due to both the presence of cold air anomalies northwest of the ETC as well as larger moisture anomalies embedded within the ETC's warm sector (Fig. 12). The stronger baroclinic environment and upper-level dynamics associated with node [3, 1] (Figs. 11 and 12) also explain why node [3, 1] features the fastest 10-m wind speeds near the ETC center compared to nodes [2, 1] and [1, 1] (Fig. 16).

Focusing on the increasingly more dynamic environments associated with the Southern Plains cyclone cluster, the presence of strong 700-hPa ascent, strong baroclinicity, and highly anomalous moisture (Figs. 11 and 12) in these nodes promote widespread precipitation north and east of the ETC center (Fig. 13). This cluster is the wettest in aggregate, with distinct rain accumulations focused near the ETC's implied warm front and snow accumulations northwest of the ETC center (Figs. 14 and 15). Within the cluster, as node environments progressively feature stronger upward vertical motion, larger north–south temperature gradients,

FIG. 15. Average ETC-centered precipitation rate resulting from snow (blue shading; mm day^{-1}) at the lowest pressure time for each node, with MSLP overlaid (black solid lines contoured every 4 hPa). The ETC center is denoted with a black L symbol. SOM clusters are outlined with colored boxes as in Fig. 7. Plotted variables are smoothed following the methodology in Fig. 7.

and larger moisture anomalies, increased impacts from precipitation and surface winds are observed, with the strongest wind speeds observed on the southwest flank of the ETC center (Fig. 16).

Returning to the bottom row of the SOM (nodes [3, 0], [3, 1], [3, 2], and [3, 3]), these four nodes generally experience the most impactful precipitation and winds. Moving from [3, 0] to [3, 3], the upper-level flow structure evolves from featuring more zonal flow (node [3, 0]) toward stronger flow curvature and along-flow speed changes, facilitating increased midlevel ascent (Fig. 11). Additionally, the synoptic environments become

progressively more baroclinic as cold air anomalies from the north extend toward the center of the study region (Fig. 12). Areas of anomalous moisture also become more consolidated within the ETC's warm sector (Fig. 12) and, paired with stronger warm-air advection in the vicinity of the ETC, contribute to more precipitation (Fig. 13). Since anomalous dry air is prominent southwest of the ETC in all four of these nodes (Fig. 12), there is no or weak precipitation observed in that location relative to the ETC (Fig. 13). The interface between dry anomalies and the anomalously moist environment northeast of the ETC also establishes an environment that potentially favors more
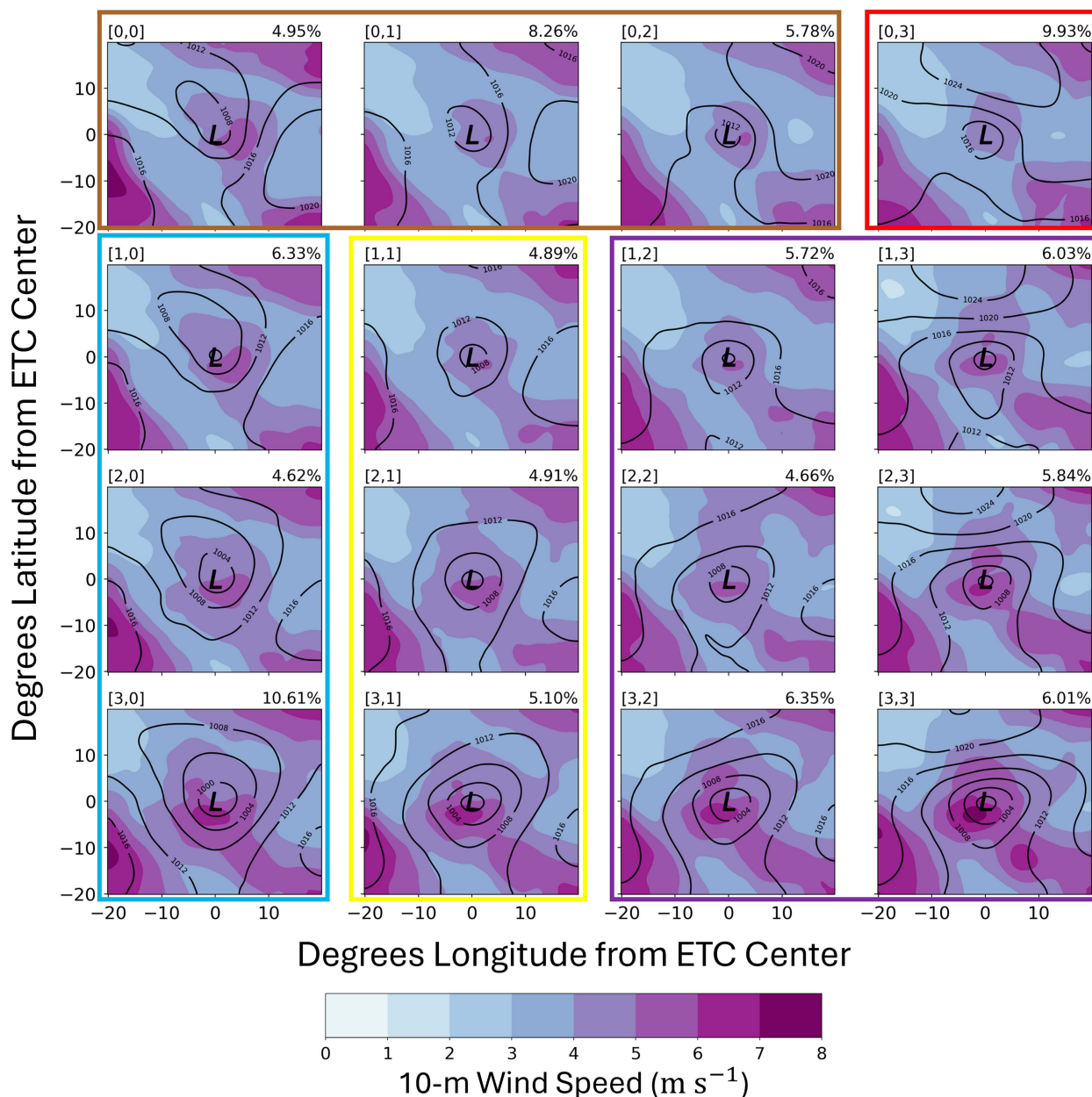
FIG. 16. Average ETC-centered 10-m wind speed (shaded according to the fill pattern; m s^{-1}) at the lowest pressure time for each node, with MSLP overlaid (black solid lines contoured every 4 hPa). The ETC center is denoted with a black L symbol. SOM clusters are outlined with colored boxes as in Fig. 7. Plotted variables are smoothed following the methodology in Fig. 7.

instability at those locations and thus more robust precipitation production.

5. Discussion and conclusions

This study examines 4723 central U.S. ETCs during October–May 1980–2021 that develop leeward of the Continental Divide. These ETCs are further partitioned into a top 20% ETC category based on the magnitude of their accompanying MSLP anomalies ($N = 945$), which represent the most anomalous

ETCs in this region. Annual, seasonal, and monthly ETC frequencies are explored, along with preferred ETC locations. To investigate the variability of central U.S. cyclones, a self-organizing map is used to classify ETC environments into 16 nodes and five synoptically meaningful clusters. Additionally, the annual and monthly ETC frequencies are examined for each node. Upper- and lower-tropospheric composite analyses provide further insight into the dynamical drivers for vertical motion and precipitation for each node, and typical precipitation types and amounts for each node are evaluated

using ETC-centered composites. Additional emphasis is placed on the bottom row of the SOM, as these nodes featured some of the most favorable dynamical and thermodynamic environments for the development of central U.S. ETCs and concomitant precipitation. The majority of top 20% ETCs are generally associated with the favorable dynamical and thermodynamic environments that characterize the nodes on the bottom row of the SOM.

Bentley et al. (2019) and Fritzen et al. (2021) found the central United States to be a frequency maximum for cyclogenesis, with Colorado and Bighorn lows being the dominant ETC types. In contrast to our study, Fritzen et al. (2021) noted a significant decrease in Colorado cool-season (October–April) ETC frequency during 1979–2019 ($r = -0.065$, $p = 0.03$). However, the frequency of Bighorn lows exhibited no significant frequency trends over the study period. Fritzen et al. (2021) utilized stricter criteria for ETC identification compared to our study (i.e., 24-h lifetime requirement, a total track distance over 500 km, and a specified ratio between the start-to-end distance over the ETC track distance), which resulted in only 258 Colorado ETCs and 80 Bighorn ETCs throughout their 40-yr study period. Due to the more relaxed ETC identification criteria (i.e., 12-h lifetime requirement and no track length criterion), as well as choosing not to focus only on Colorado and Bighorn ETCs in the present study, we investigated more central U.S. ETCs than Fritzen et al. (2021). At the time of ETC lowest pressure, average minimum central pressure trends and top 20% ETC central pressure anomaly trends are insignificant. This result is not perfectly comparable with Fritzen et al. (2021) likely because of differences in domain sizes and ETC identification schemes between the two studies. Nevertheless, the lack of strong central pressure trends identified in this study is similar to previous work.

It is important to note that this study includes May in our definition of the cool season because the central United States—and especially Colorado—often experiences cool-season ETCs well into May (e.g., Whittaker and Horn 1981 and Wernli and Schwierz 2006). Bierly and Harrington (1995) conducted a climatology of transition season (i.e., October, November, April, and May) Colorado ETCs during 1961–90, which represents the most recent Colorado-focused ETC climatology in the peer-reviewed literature. Bierly and Harrington's (1995) inclusion of April and May ETCs as part of their climatology served as motivation for the start and end months of our cool-season climatology of lee cyclogenesis events along the Rocky Mountains. Bierly and Harrington (1995) identified 191 Colorado ETCs during the four transition months identified above, with April ETCs found to be more frequent. Conversely, Whittaker and Horn (1981) found March Colorado ETCs to be more frequent during a shorter and earlier study period (1958–77). In the present study, April ETCs across the central United States were found to be the second most common behind May, but April contained the most top 20% ETCs compared to all other cool-season months. The present study also found winter and spring ETCs to significantly contribute to the overall increase in cool-season ETC frequency over time. Bierly and Harrington (1995) found a significant

decrease in transition season Colorado ETCs over their period of study ($r = -0.53$, $p < 0.05$), with April and May ETCs contributing heavily to this decrease. While more ETCs and months are included in the present study, it was found that all central U.S. ETCs are increasing over the study period, but the most anomalous ETCs (top 20%) are not becoming more frequent. Instead, most of the trend for all ETCs is attributed to the weaker cyclones. ETC occurrence exhibits considerable year-to-year variability, however, as also noted in Bierly and Harrington (1995), which adds some uncertainty to any trends derived in this work, and may partly explain differences in trends derived as part of prior work in addition to differences in cyclone detection between studies.

Five synoptically unique clusters were defined from the SOM developed for this study: 1) the Mississippi River Valley anticyclone cluster, 2) the Canadian anticyclone cluster, 3) the Northern Plains cyclone cluster, 4) the Central Plains cyclone cluster, and 5) the Southern Plains cyclone cluster. SOMs are a versatile machine learning tool in the synoptic–dynamic community through their ability to identify different categories of events within spatially varying datasets. For example, Seefeldt et al. (2012) utilized SOMs to characterize the variability in moisture distributions across West Africa, Baiman et al. (2023) used SOMs to identify synoptic-scale drivers of atmospheric rivers in Antarctica, and LaChat et al. (2024) employed SOMs to diagnose types of Rossby wave breaking in the Northern Hemisphere. The present study found that one of the most frequent SOM nodes features a strong anticyclone over the U.S./Canadian border, which was defined as the Canadian anticyclone cluster. This cluster is one of two nodes that exhibit a significant increase in ETC frequency during the 1980–2021 study period. Few top 20% ETCs are observed in association with this node and precipitation production is not as prolific compared to nodes with enhanced baroclinicity and more anomalous moisture. The most dynamically favorable environments for ETC-generated precipitation within the SOM feature strong north–south lower-tropospheric temperature anomaly dipoles (the Southern Plains cluster and node [3, 1] in the Central Plains cluster) that result in increased baroclinicity and stronger temperature advection in the vicinity of the ETC. Paired with the presence of highly anomalous moisture, and strong synoptic-scale forcing for ascent, these nodes produce robust precipitation within the ETC's near environment. The remaining SOM clusters that do not produce as much precipitation within the SOM include the Mississippi River Valley cluster and the Northern Plains cyclone cluster. The synoptic-scale environments within these clusters are largely driven by distinct branches of the polar and subtropical jet or a prominent North Pacific jet, respectively. Given that the SOM in this study performed well in capturing the variability of central U.S. ETC types and impacts, the SOM offers the potential to inform future forecasts of central U.S. ETCs and a framework for evaluating the predictability of ETC impacts. Such an avenue is highlighted as a promising area for future work and may provide forecasters with useful guidance in predicting cool-season weather conditions across the central United States.

REFERENCES

Baiman, R., A. C. Winters, J. Lenaerts, and C. A. Shields, 2023: Synoptic drivers of atmospheric river induced precipitation near Dronning Maud Land, Antarctica. *J. Geophys. Res. Atmos.*, **128**, e2022JD037859, https://doi.org/10.1029/2022JD037859.

Bannon, P. R., 1992: A model of Rocky Mountain lee cyclogenesis. *J. Atmos. Sci.*, **49**, 1510–1522, https://doi.org/10.1175/1520-0469(1992)049<1510:AMORML>2.0.CO;2.

Bentley, A. M., L. F. Bosart, and D. Keyser, 2019: A climatology of extratropical cyclones leading to extreme weather events over central and eastern North America. *Mon. Wea. Rev.*, **147**, 1471–1490, https://doi.org/10.1175/MWR-D-18-0453.1.

Bierly, G. D., and J. A. Harrington, 1995: A climatology of transition season Colorado cyclones: 1961–1990. *J. Climate*, **8**, 853–863, https://doi.org/10.1175/1520-0442(1995)008<0853:ACOTSC>2.0.CO;2.

Browning, K. A., 1997: The dry intrusion perspective of extratropical cyclone development. *Meteor. Appl.*, **4**, 317–324, https://doi.org/10.1017/S1350482797000613.

Bureau, 2024: 2020 census urban areas facts. https://www.census.gov/programs-surveys/geography/guidance/geo-areas/urban-rural/2020-ua-facts.html.

Cassano, E. N., J. M. Glisan, J. J. Cassano, W. J. Gutowski Jr., and M. W. Seefeldt, 2015: Self-organizing map analysis of widespread temperature extremes in Alaska and Canada. *Climate Res.*, **62**, 199–218, https://doi.org/10.3354/cr01274.

Clark, J. H. E., 1990: An observational and theoretical study of Colorado lee cyclogenesis. *J. Atmos. Sci.*, **47**, 1541–1561, https://doi.org/10.1175/1520-0469(1990)047%3C1541:AOATSO%3E2.0.CO;2.

Davis, C. A., 1997: The modification of baroclinic waves by the Rocky Mountains. *J. Atmos. Sci.*, **54**, 848–868, https://doi.org/10.1175/1520-0469(1997)054%3C0848:TMOBWB%3E2.0.CO;2.

Dunn, L., 1987: Cold air damming by the front range of the Colorado Rockies and its relationship to locally heavy snows. *Wea. Forecasting*, **2**, 177–189, https://doi.org/10.1175/1520-0434(1987)002%3C0177:CADBTF%3E2.0.CO;2.

Dunn, L. B., 1992: Evidence of ascent in a sloped barrier jet and an associated heavy-snow band. *Mon. Wea. Rev.*, **120**, 914–924, https://doi.org/10.1175/1520-0493(1992)120%3C0914:EOAIAS%3E2.0.CO;2.

Fawcett, E. B., and H. K. Saylor, 1965: A study of the distribution of weather accompanying Colorado cyclogenesis. *Mon. Wea. Rev.*, **93**, 359–367, https://doi.org/10.1175/1520-0493(1993)093<0359:ASOTDO>2.3.CO;2.

Fritzen, R., V. Lang, and V. A. Gensini, 2021: Trends and variability of North American cool-season extratropical cyclones: 1979–2019. *J. Appl. Meteor. Climatol.*, **60**, 1319–1331, https://doi.org/10.1175/JAMC-D-20-0276.1.

Harman, J. R., 1991: *Synoptic Climatology of the Westerlies: Process and Patterns.* Association of American Geographers, 80 pp.

Hersbach, H., and Coauthors, 2023: ERA5 hourly data on pressure levels from 1940 to present. Copernicus Climate Change Service (C3S) Climate Data Store (CDS), accessed 26 September 2025, https://doi.org/10.24381/cds.adbb2d47.

Kohonen, T., 1982: Self-organized formation of topologically correct feature maps. *Biol. Cybernetics*, **43**, 59–69, https://doi.org/10.1007/BF00337288.

——, 2001: *Self-Organizing Maps.* Springer Series in Information Sciences, Vol. 30, Springer, 502 pp., https://doi.org/10.1007/978-3-642-56927-2.

LaChat, G., K. A. Bowley, and M. Gervais, 2024: Diagnosing flavors of tropospheric Rossby wave breaking and their associated dynamical and sensible weather features. *Mon. Wea. Rev.*, **152**, 513–530, https://doi.org/10.1175/MWR-D-23-0153.1.

Marshment, R. A., and L. H. Horn, 1986: Spring season Colorado cyclones. Part II: Composites of atmospheric moisture and moist static stability. *J. Climate Appl. Meteor.*, **25**, 744–752, https://doi.org/10.1175/1520-0450(1986)025<0744:SSCCPI>2.0.CO;2.

NWS, 2024: March13–14 2021 Northeast Colorado blizzard. NOAA's National Weather Service, https://www.weather.gov/bou/March13_14_2021NortheastColoradoBlizzard#:~:text=A%20significant%20blizzard%20struck%20northeast,Colorado%20on%20Sunday%2C%20March%2014.

Newton, C. W., 1956: Mechanisms of circulation change during a lee cyclogenesis. *J. Atmos. Sci.*, **13**, 528–539, https://doi.org/10.1175/1520-0469(1956)013%3C0528:MOCCDA%3E2.0.CO;2.

Palmén, E., and C. W. Newton, 1969: Preface. *Atmospheric Circulation Systems: Their Structure and Physical Interpretation*, International Geophysics, Vol. 13, Elsevier, v–viii, https://doi.org/10.1016/S0074-6142(08)62791-6.

Sammon, J., 1969: A nonlinear mapping for data structure analysis. *IEEE Trans. Comput.*, **C-18**, 401–409, https://doi.org/10.1109/T-C.1969.222678.

Seefeldt, M. W., T. M. Hopson, and T. T. Warner, 2012: A characterization of the variation in relative humidity across West Africa during the dry season. *J. Appl. Meteor. Climatol.*, **51**, 2077–2089, https://doi.org/10.1175/JAMC-D-11-0196.1.

Sprenger, M., and Coauthors, 2017: Global climatologies of Eulerian and Lagrangian flow features based on ERA-Interim. *Bull. Amer. Meteor. Soc.*, **98**, 1739–1748, https://doi.org/10.1175/BAMS-D-15-00299.1.

U.S. Department of Commerce, 2024: History of snowfall observations at Denver. NOAA's National Weather Service, https://www.weather.gov/bou/SeasonalSnowfall.

Wernli, H., and C. Schwierz, 2006: Surface cyclones in the ERA-40 dataset (1958–2001). Part I: Novel identification method and global climatology. *J. Atmos. Sci.*, **63**, 2486–2507, https://doi.org/10.1175/JAS3766.1.

Whittaker, L. M., and L. H. Horn, 1981: Geographical and seasonal distribution of North American cyclogenesis, 1958–1977. *Mon. Wea. Rev.*, **109**, 2312–2322, https://doi.org/10.1175/1520-0493(1981)109<2312:GASDON>2.0.CO;2.